Overload Behavior of an Experimental Precast Prestressed Concrete Segmental Bridge

Mohamed Abdel-Halim
Assistant Professor of Civil Engineering
Yarmouk University
Irbid, Jordan

Richard M. McClure
Associate Professor of Civil Engineering
The Pennsylvania State University
University Park, Pennsylvania

Harry H. West
Professor of Civil Engineering
The Pennsylvania State University
University Park, Pennsylvania

In recent years, interest in segmental bridges has grown and their behavior under applied loads has received much attention. The Pennsylvania Department of Transportation, with the support of the Federal Highway Administration, responded to this growing interest by sponsoring the construction of an experimental segmental bridge as a part of the 1 mile (1.6 km) oval shaped test track which is operated by the Pennsylvania Transportation Institute at The Pennsylvania State University.

One of the objectives of this research was to study the overload behavior in order to establish actual safety factors. This required loading the bridge to failure in addition to conducting theoretical studies. An analytic procedure based on the finite element method was developed to predict the complete load-deformation response of the prestressed segmental bridge. The girder was also analyzed using the standard theoretical analysis for prestressed concrete structures, which is a simpler method. The theoretical results obtained by those two methods were then compared with the experimental results from the failure tests.

Synopsis

An experimental prestressed concrete segmental bridge was constructed and tested at the Pennsylvania Transportation Institute of The Pennsylvania State University.

The bridge was designed by the Pennsylvania Department of Transportation as two independent single-span curved girders with a length of 121 ft (36.9 m). Each girder was composed of seventeen segments. The bridge was initially field tested at service load levels and subsequently tested for overloads when one girder was tested to failure.

The incremental loading to failure is discussed and these results are compared with those obtained from a finite element analysis (SAP IV), which models the cracking patterns and material nonlinearities. In addition, the results of classical simplified analyses are compared with selected experimental and finite element results.

Conclusions are given that relate to the application of the research.

TEST BRIDGE

The general plan, elevation, and cross section of the experimental bridge are shown in Fig. 1. The bridge consisted of two identical simply supported girders with segments and joints numbered as shown. Each independent girder consisted of seventeen segments which were tied together with longitudinal bar or strand post-tensioning tendons plus diagonal bar post-tensioning tendons. The ducts containing the tendons were grouted after post-tensioning. Steel shear dowels were used to achieve alignment during construction and to transfer torsional moment after the girders were built. Epoxy was used as the main jointing material between the segments.

End diaphragms were introduced in the end segments, which were ample in size to take the substantial reaction forces from the neoprene bearing pads and torsional anchorages and to provide room for the post-tensioning end anchorage plates. In addition, an opening was made to allow easy access by researchers to the inside of the box section. An open longitudinal joint between the girders was selected to allow an independent comparison of the two girders. The overload tests were performed on Girder B.

The segments for the experimental bridge were cast individually at a fabrication plant by the short line method in one steel form with provisions for adjustments. They were then hauled about 100 miles (161 km) to the test track facility where they were erected on steel scaffolding-type falsework.

The curved box girder was designed for longitudinal moment using straight beam theory for the dead load, AASHTO HS20-44 live loading, and prestress. The design was made using allowable stresses and checked for ultimate strength. For transverse moment, the segments were designed elastically as a box frame with side cantilever flanges. At the bottom of the webs the frame was assumed to be simply supported. Each girder was analyzed for torsion as a horizontally curved beam with eccentric loads. The cross section of the segments was approximated as a box section with the flanges neglected.

The design strength of the concrete at 28 days was 5750 psi (39.6 N/mm^2). Intermediate grade ASTM A615 reinforcing bars with a specified minimum yield stress of 40,000 psi (275 N/mm^2) were used for all mild steel reinforcement. Post-tensioning steel bars with a specified ultimate stress of 160,000 psi (1100 N/mm^2), or steel strand with a specified ultimate stress of 270,000 psi (1860 N/mm^2), were used for all post-

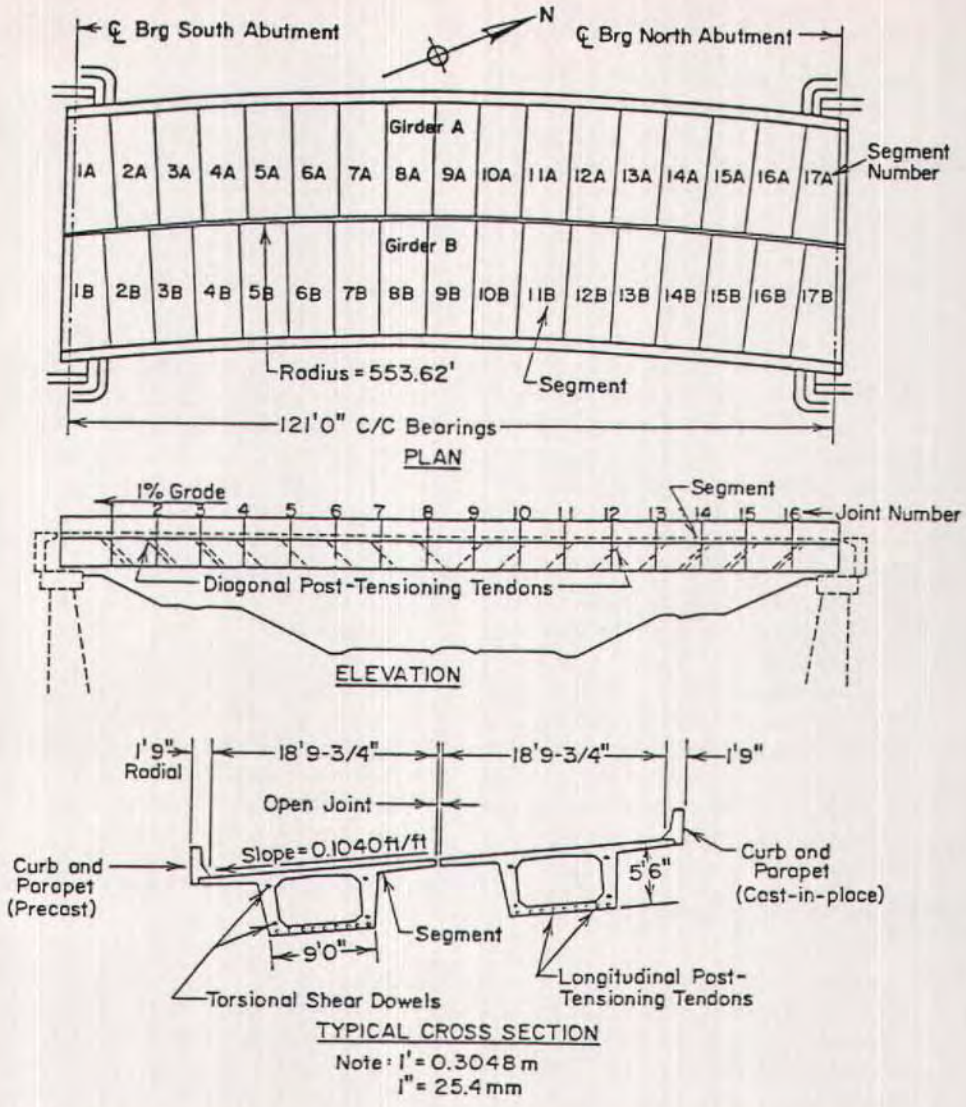

Fig. 1. General plan, elevation and typical section of an experimental segmental bridge.

tensioning tendons.

In order to take into consideration the effect of time on the strength of concrete, concrete cylinders were tested before the bridge was loaded to failure. Some of these cylinders were tested for compressive strength, static modulus of elasticity, and Poisson's ratio, and others were tested for splitting tensile strength.

Table 1 gives the properties for the concrete in Girder B at the time of testing. Specimens of the 0.50 in. (13 mm) diameter strands and of the 1.25 in. (32 mm) stress steel bars were tested by the manufacturer and the Pennsylvania Department of Transportation. The results are also given in Table 1.

Complete details and design criteria

Table 1. Material properties.

Properties of concrete		
Age (year)		4.5
Compressive strength (psi)		7,350
Tensile strength (psi)		646
Modulus of elasticity (psi)		5,232,000
Poisson's ratio		0.189
Properties of prestressing bars and strands		
	Bars	Strands
Diameter (in.)	1.25	0.50
Yield strength (ksi)	156.5	256.0
Ultimate strength (ksi)	169.6	283.7
Modulus of elasticity (ksi)	30,555.	28,000.
Percent of elongation	5.5	6.4

Note: 1 in. = 25.4 mm; 1 ksi = 6.895 N/mm.²

for the test bridge can be found in the final report on Research Project 72-9, Penn DOT Publication No. 118.[1]

FINITE ELEMENT ANALYSIS

Modeling of Materials

Concrete in the bridge has complex stress distributions resulting from a number of sources. Success in analyzing such a structure requires knowledge of the deformational behavior and strength properties of concrete under multiaxial states of stress. Different models based upon different theories have been proposed for the stress-strain law of concrete under short-term loads. These are based on plasticity, nonlinear elasticity, model of microstructures, measure of damage, endochronic theory of plasticity, and mathematical functions. A complete explanation of all these models can be found in Ref. 2.

After examining these various models, it was concluded that, until more extensive and appropriate investigations become available, a type of model that allows a direct inclusion of the experimental data should be preferred. Therefore, Kostovos and Newman's model[3-6] was chosen for the analysis of the bridge.

Octahedral Stresses and Strains

It was assumed in this work that compressive stresses and strains were positive and that σ_1, σ_2, and σ_3 represent the maximum, intermediate, and minimum principal stresses, respectively. The orthogonal coordinate system σ_1, σ_2, and σ_3, which defines the stress space, was transformed into a cylindrical coordinate system in which z coincides with the space diagonal ($\sigma_1 = \sigma_2 = \sigma_3$) of the original system, and r and θ are the radius and rotational variables, respectively, on the plane perpendicular to the z axis (octahedral plane), as shown in Fig. 2.

The two coordinate systems are related by the following equations:

$$z = (\sigma_1 + \sigma_2 + \sigma_3)/\sqrt{3} = \sqrt{3}\,\sigma_o \quad (1)$$

$$r = (1/\sqrt{3}) \times \sqrt{(\sigma_1 - \sigma_2)^2 + (\sigma_2 - \sigma_3)^2 + (\sigma_3 - \sigma_1)^2} = \sqrt{3}\,\tau_o \quad (2)$$

$$\cos\theta = \frac{\sigma_1 + \sigma_2 - 2\,\sigma_3}{r\sqrt{6}} \quad (3)$$

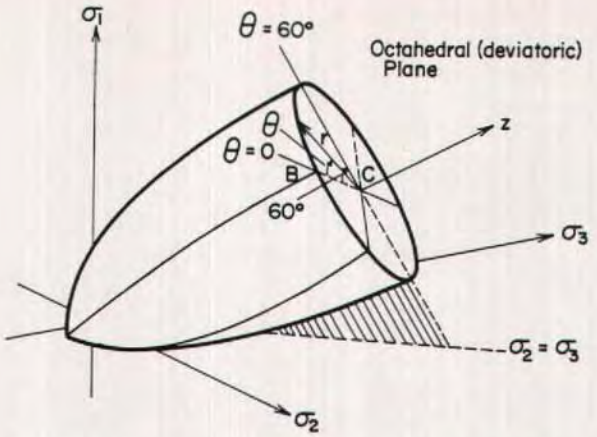

Fig. 2. Schematic representation of the ultimate strength surface.

In these equations, σ_o and τ_o are known as the normal and the shear octahedral stresses, respectively.

Similarly, the normal (ϵ_o) and shear (γ_o) octahedral strains are defined as follows:

$$\epsilon_o = (\epsilon_1 + \epsilon_2 + \epsilon_3)/3 \tag{4}$$

$$\gamma_o = \tfrac{1}{3}\sqrt{(\epsilon_1 - \epsilon_2)^2 + (\epsilon_2 - \epsilon_3)^2 + (\epsilon_3 - \epsilon_1)^2} \tag{5}$$

Here, ϵ_1, ϵ_2, ϵ_3 are the strains in the directions of the principal stresses. If elastic behavior is assumed, the stress σ_o and strain ϵ_o associated with volume change are related by the bulk modulus K, and the distortional quantities are related by the shear modulus G as:

$$K = \frac{E}{3(1-2\nu)} = \frac{\sigma_o}{3\epsilon_o} \tag{6}$$

$$G = \frac{E}{2(1+\nu)} = \frac{\tau_o}{2\gamma_o} \tag{7}$$

For nonlinear materials, Kostovos and Newman used similar relationships, but in this case, the moduli K and G are functions of stress and strain, and can be expressed as secant moduli in the form:

$$K_s(\sigma_o) = \frac{\sigma_o}{3\epsilon_o(\sigma_o)} \tag{8}$$

$$G_s(\tau_o) = \frac{\tau_o}{2\gamma_o(\tau_o)} \tag{9}$$

Concrete in Compression

In their work, Kostovos and Newman have shown that concrete compression behavior and fracture characteristics may be explained by the formation and propagation of microcracks within the concrete. Under applied loading, four stages of behavior can be distinguished in the stress-strain response for uniaxial, biaxial and triaxial stress cases. Consider, as an example, the stress-strain curve for uniaxial compression which is shown in Fig. 3.

As a first stage, consider the region up to 30-60 percent of the ultimate strength (shown as 45 percent in Fig. 3). In this initial stage (Stage 1 in Fig. 3), microcracks in addition to those preexisting in the material are initiated at isolated points where the tensile strain concentrations are the highest. However, these cracks are completely stable. Localized cracks are initiated but they do not propagate.

A second stage (Stage II, in Fig. 3), takes the region up to 70-90 percent of the ultimate strength. As the applied load is increased, the crack system mul-

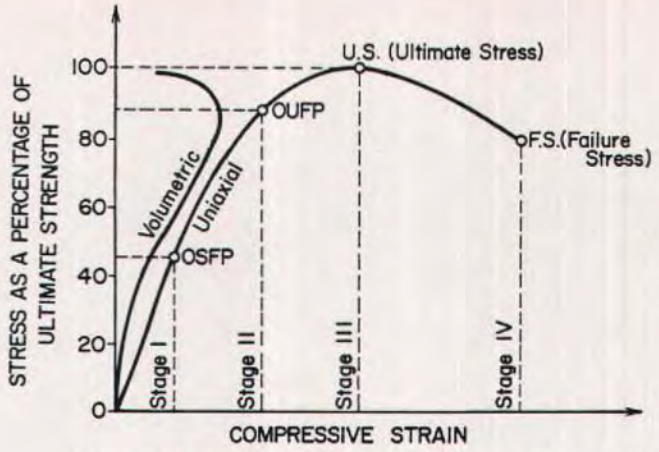

Fig. 3. Uniaxial stress-strain curve for concrete.

tiplies and propagates, but in a slow stable manner. If loading is stopped and the stress level is maintained at a certain value, crack propagation ceases. The increasing internal damage, revealed by deviation of the linear elastic behavior, causes irrecoverable deformation upon unloading. The start of such deformation behavior has been termed "onset of stable fracture propagation" (OSFP).

A third stage (Stage III in Fig. 3) applies up to the ultimate strength. Interface microcracks are linked to each other by mortar cracks, and void formation (dilation) begins to have its effect on deformation. The start of this stage has been termed "onset of unstable fracture propagation" (OUFP). The level is easily defined since it coincides with the level at which the overall volume of the material becomes a minimum.

A fourth stage defines the region beyond the ultimate strength. In this region (Stage IV in Fig. 3), the energy released by the propagation of a crack is greater than the energy needed for propagation. Thus, the cracks become unstable and self-propagating until complete disruption and failure occurs.

Similarly, the multiaxial behavior model of Kostovos and Newman has considered four stages which will be explained in the following sections.

Elastic Concrete (Stage I) — Under combined states of stress, the stress-strain relationship is generally nonlinear. However, when stress is below 45 percent of the ultimate stress, the material characteristics are unaffected by the fracture processes explained previously, the deformation is recoverable, and the stress-strain relationship is almost linear. Therefore, it is assumed here that concrete is isotropic, homogeneous, linearly elastic, and that its stress-strain relations are described completely by two elastic constants, Poisson's ratio (ν) and Young's modulus (E).

Inelastic Concrete (Stage II) — This stage represents states of stress between 45 percent of the ultimate stress, which has been termed the "onset of stable fracture propagation" (OSFP), and 85 percent of the ultimate stress, which has been termed the "onset of unstable fracture propagation" (OUFP). In this zone of behavior, Kostovos and Newman consider deformations to be composed of the following components:

1. A component dictated by the materials characteristics and unaffected by the fracture process.[5]

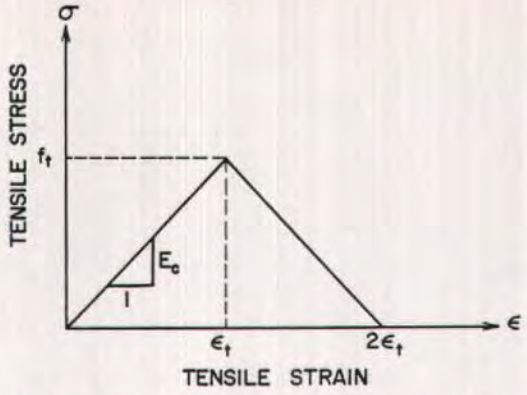

Fig. 4. Assumed stress-strain curve for concrete in tension.

2. A component expressing the effect of internal stresses caused by the fracture processes.

Relationships between σ_o and ϵ_o, and between τ_o and γ_o have been expressed using the experimental results. These relationships were formulated as follows:

$$\epsilon_o = f_1(\sigma_o) \tag{10}$$

$$\gamma_o = f_2(\tau_o) \tag{11}$$

Then, the secant expressions of the bulk and shear moduli, given by Eqs. (8) and (9), can be calculated. After that, the secant values of the modulus of elasticity E and Poisson's ratio ν were obtained from the well-known formulas of linear elasticity:

$$E = \frac{9KG}{3K + G} \tag{12}$$

$$\nu = \frac{3K - 2G}{2(3K + G)} \tag{13}$$

Inelastic Concrete (Stage III) — This stage represents states of stress between the OUFP and the ultimate strength levels. In this zone, void formation begins to have an effect. Therefore, the deformations that occur in this stage are considered to be composed of three components: the two components explained in the previous section plus a third component which expresses the effect of void formation.[4] The addition of the void formation effect to the first two components gives the total deformations. Then, the secant values of the modulus of elasticity E and Poisson's ratio ν were obtained following the same steps explained in Stage II.

Inelastic Concrete (Stage IV) — This stage represents states of stress beyond the ultimate strength level. In this zone, the volume of voids increases dramatically, which causes rapid dilation of the overall volume. At this point, it is evident that the specimen, or the concrete element as a whole, can no longer be considered as a continuum. However, an attempt has been made to use the work of Kostovos and Newman[6] concerning the behavior of concrete beyond the ultimate strength level. Here, the effect of the voids beyond the ultimate strength has been added to the deformations at the ultimate level to obtain the total deformations, that is:

$$\epsilon_o = \epsilon_o^u + \delta\epsilon_o \tag{14}$$

$$\gamma_o = \gamma_o^u + \delta\gamma_o \tag{15}$$

Here $\delta\epsilon_o$ and $\delta\gamma_o$ are the hydrostatic and deviatoric components of the voids deformations beyond ultimate, respec-

tively. And, ϵ_o^u and γ_o^u are the hydrostatic and deviatoric components at ultimate, respectively.

Concrete in Tension

For concrete in tension, it can be assumed without significant loss of accuracy that linear behavior is obtained up to cracking.[7] Therefore, the stress-strain relationship has been described by two elastic constants, Poisson's ratio (ν) and Young's modulus (E). The tensile strength for the concrete in triaxial tension, or in the tension-tension-compression quadrant, was taken to be equal to its uniaxial tensile strength.

The concrete stress is zero at the cracks, but it is not zero if averaged over the distance between cracks. Thus, if the concept of working with average stress is considered, an unloading portion of the stress-strain curve can be assumed. No data are available concerning the unloading portion of the curve. Therefore, the stress-strain curve for concrete in tension was taken as shown in Fig. 4. The modulus of elasticity for any tensile strain is taken as the secant modulus for that point on the curve.

Modeling of the Cracked Elements

The stiffness of the cracked elements was softened isotropically. This softening was taken into consideration by reducing the modulus of elasticity (E) according to the assumed stress-strain curve for concrete in tension shown in Fig. 4. Some shear stiffness was retained in the cracked elements. Hand et al.[8] show that although retention of some shear stiffness is necessary, the proportion of shear stiffness retained, β, is not critical, i.e., various values of β resulted in similarly good correlation with test results.

Modeling of the Prestressing Steel

An elastic strain hardening model was used in defining the material behavior of the prestressing steel. The strain hardening of the material was defined according to the experimental stress-strain curve.

Modeling of the Mild Steel Reinforcement

The cross section of the bridge is heavily reinforced with mild steel reinforcement. In order to account for its existence, the mild steel reinforcement was uniformly distributed throughout the concrete elements, and new effective values for the modulus of elasticity were established for individual regions of the cross section, with each region encompassing a portion of the cross section where the reinforcing pattern was fairly uniform.

General Technique Used for the Nonlinear Analysis

Nonlinearity is caused solely by the nonlinear form of the constitutive relations and failure laws of concrete and steel. Strains are assumed to be small and, thus, the strain-displacement relations are linear. Therefore, the problem involves material nonlinearity only, and a nonlinear solution must satisfy the constitutive laws and the conditions of equilibrium and compatibility within an acceptable margin of error.

The procedure used for the analysis was as follows:

(a) Discretize the structure into elements by introducing the finite element grid, number the nodes, and number the elements. The centroidal characteristics of each element are considered in all calculations to represent the average properties of that element. Apply an initial load, and carry out an elastic analysis using a linear finite element program (SAP IV in this study) to obtain the nodal displacements and element stresses. Calculate the corresponding principal stresses. Use a scaling factor to raise the load level to cause first cracking in an element or region of elements. Then, linearly scale the nodal displace-

ments and element stresses to yield their respective values at the cracking load of the structure.

(b) Modify the material properties of the cracked elements to account for tension stiffening of the concrete. The load is then increased by increments of varying magnitude, with each cycle of loading reflecting the changing properties of the materials.

The following computational steps were involved in a typical cycle of loading:

1. Increase the previous load by an increment of loading ($P_i = P_{i-1} + \Delta P_{i-1}$). Perform an elastic analysis for the structure under load P_i, using the updated stiffness matrix at the end of the previous load. That is, if $[K]_{i-1}$ is the updated stiffness matrix at the end of load P_{i-1}. Then:

$$\{P\}_i = [K]_{i-1}\{\Delta\}_i$$

where $\{P\}_i$ and $\{\Delta\}_i$ are the load vector and displacement vector for general system at cycle i, respectively. Calculate nodal displacements $\{\Delta\}_i$ and element stresses.

2. Calculate the corresponding principal stresses.

3. Check concrete cracking and inelasticity and check steel inelasticity.

4. Examine the stress level for each inelastic concrete element. Then define the stage of behavior for each inelastic element.

5. Modify the material properties of these inelastic elements.

6. Modify the material properties of the old and new cracked elements to account for tension stiffening of the concrete and modify the steel properties using its experimental stress-strain diagram.

7. Update the structure stiffness at the end of the load P_i, using the new material properties in preparation for the next load level.

This computational cycle was repeated until the ultimate load was reached and the complete behavior of the structure was determined in terms of displacements, stresses, and crack patterns for each desired load.

In checking for cracking, it is important to note that when the calculated tensile stress, σ_1, in any element is higher than the ultimate tensile strength of the concrete, f_t, the stresses in all the elements must be scaled down to remove the stress increment ($\sigma_1 - f_t$), and the load and nodal displacements must also be scaled down to yield their respective values.

It is important to mention that the stresses (forces) released from the cracked elements in cycle i, for example, will be redistributed to the neighboring elements in the next cycle, cycle ($i + 1$).

Use of SAP IV

SAP IV is a finite element structural analysis program for the static and dynamic response of linear structural systems. The program is written in FORTRAN. The user's manual[9] describes the logical construction of the program, the analysis capabilities, the finite element library and the input data.

Two of the elements were used for the bridge problem. The three-dimensional truss element was used to represent the lumped prestressing tendons, and the three-dimensional solid (eight-node brick) element to represent the concrete.

Discretization of the Structure

Nodes and subdivision lines and planes were located at positions where there were abrupt changes in geometry, changes in material properties, changes in prestressing tendons, and points of loadings. Figs. 5 and 6 show the longitudinal and cross-sectional discretization of the structure, respectively.

The precise arrangement for the prestressing steel was not modeled because it would have required too many node points. Instead, tendons were lumped together and the cross-sectional areas of

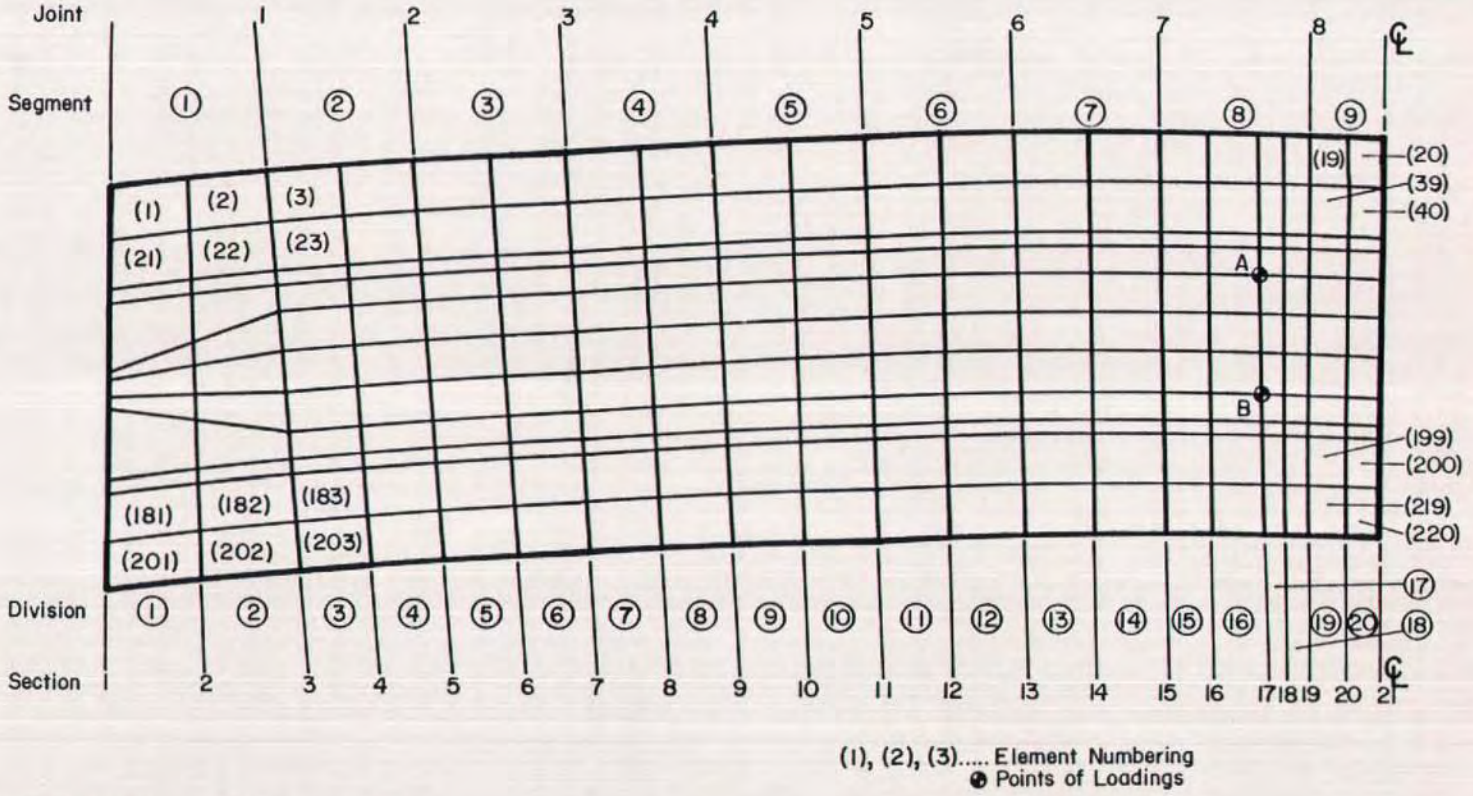

Fig. 5. Longitudinal discretization pattern.

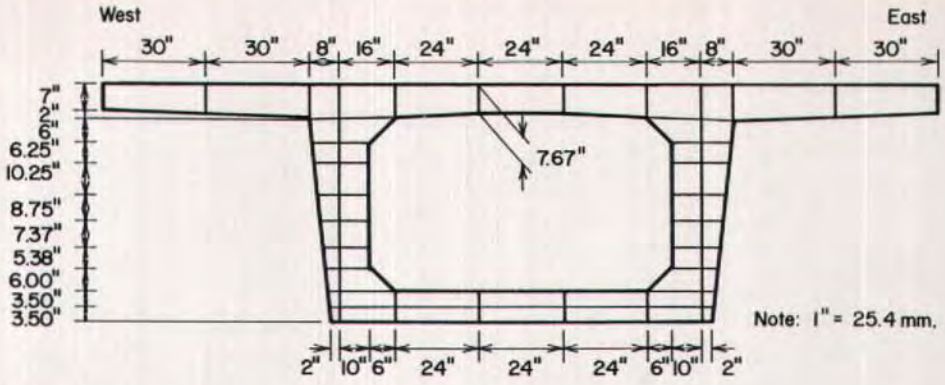

Fig. 6. Typical discretization for interior section.

certain truss members were given different values along the beam, depending on the areas of steel lumped in each division. The effective values of the modulus of elasticity for these truss members were used where appropriate.

Symmetry was used in the analysis of the bridge with one-half of the total structure represented by finite elements.

Prestressing Analysis

The material properties of concrete and steel depend on the stress or strain state of the material. The state of stress in a prestressed concrete element is produced by the prestressing forces and loads applied to the structure. Therefore, at any state of loading, stresses caused by prestressing forces should be calculated and added to those caused by the applied loads in order to define the material properties of the element.

The force that a tendon will exert upon the structure is a function of several variables. The most important of these are the jacking forces, P_j, applied at the anchors, losses of prestressing force, and position and geometry of the tendon. In this study, the effects of all these variables were taken into account. The time-dependent losses were calculated in detail according to standard procedures[10] and the equivalent load method[10,11] was used to compute the forces applied by the tendons on the structure.

The effective prestress force after losses are accounted for is called P_e. These effective prestressing forces were represented as nodal forces on the finite element model. The effects of the change in the vertical alignment of the prestressing tendons and the horizontal curvature in the beam axis were considered in this representation.

The initial stresses in the bars and tendons, caused by the effective prestressing forces P_e, were calculated by dividing the force $P_e + \Delta P_{e,s}$, in any bar, by the cross-sectional area of that bar. Here, $\Delta P_{e,s}$ is the force caused by elastic shortening, and it was added to correct for the elastic shortening effect which takes place when the effective prestressing forces are applied as nodal forces on the finite element nodel.

Cases of Loading

The cases of loading needed in the analysis procedure are defined as follows:

— Experimentally, the deflections and surface strains due to live load (LL) only were measured. Thus, to compare these experimental results, theoretical

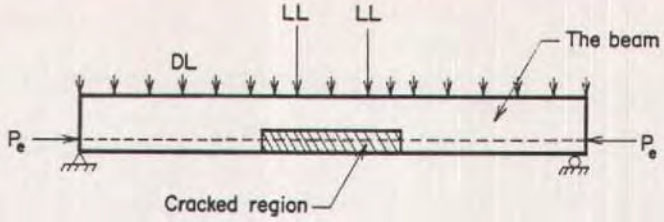

(a) Load case 1, cracked beam

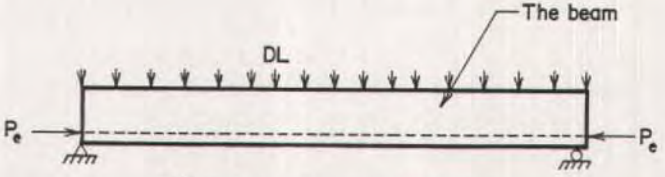

(b) Load case 2, uncracked beam

Fig. 7. Cases of loadings for cracked and uncracked beams.

deflections and surface strains due to (LL) only are needed.

— To define the material properties after any load increment, the total stresses due to live load (LL), dead load (DL), and prestressing force, P_e, in the concrete and steel elements, are needed.

Therefore, two load cases, as shown in Fig. 7, were used after each load increment. Load case 1 was used to find the total stresses needed to define the material properties. For concrete, the stresses obtained from the results of load case 1 were used directly to define the material properties for the concrete elements. However, for the steel, the initial stresses caused by $P_e + \Delta P_{e.s}$ forces were added to those obtained from the output of load case 1 to obtain the total stresses in the steel due to P_e + LL + DL. Here, the term $\Delta P_{e.s}$ is added to negate the elastic shortening effect which occurs to the steel, due to P_e, in load case 1.

Deflections and surface strains due to live load only were obtained by subtracting the results of load case 2 from the results of load case 1.

PROCEDURES FOR ANALYZING PRESTRESSED CONCRETE STRUCTURE

This procedure was used to calculate moment-curvature relationships at different load levels. Theoretical deflections were then calculated by loading the conjugate beam with the curvature diagram. The girder was idealized as a straight line structure which had the same geometry as the centroid of the cross section and torsion was neglected in the analysis.

The following assumptions were used in this analysis procedure:

1. Complete bond was assumed between tendons and concrete. Therefore, changes in strain in the steel and concrete were assumed to be the same.
2. After first cracking, tension in the concrete was neglected.
3. Strains at the various section levels were assumed to be directly proportional to the distance from neutral axis.
4. The actual stress-strain diagrams for the prestressing bars and strands were used in the analysis.

5. At ultimate strength, the maximum moments and curvatures were calculated using the rectangular stress distribution for the concrete and an ultimate strain of 0.003.

Up to First Cracking

The total moment causing cracking was found by setting the concrete stress at the bottom face, due to all loads plus the prestress force, equal to the modulus of rupture of the concrete.

For moments smaller than the cracking moment, there was an uncracked section and the stresses were in the elastic range. The curvature was calculated from the strain diagram and stress due to all loads plus prestress force calculated using the combined axial force plus bending moment equation.[10]

After First Cracking

For cracked prestressed concrete beams, calculation of stresses after cracking is a complex matter. The neutral axis location and effective section properties depend not only on the geometry of the cross section and the material properties, as for reinforced concrete beams, but also on the axial prestressing force and the loading. The axial force applied by the steel to the concrete is not constant after cracking, but depends on the loading and on the section properties. Nilson[10] has developed a method for calculating flexural stresses in prestressed beams after cracking. This method works for stresses in the elastic and inelastic ranges but a complete stress-strain diagram for all materials must be known.

Ultimate Flexural Strength

The ultimate strength of the girder was determined by the strain compatibility method using stress-strain diagrams of the prestressing tendons. A complete explanation of the strain compatibility method has been given by Nilson.[10]

BRIDGE TESTING

The Loading System

The bridge was tested with static loading using the loading frames shown in Fig. 8. The loading frame included four hydraulic jacks. Directly above the rock anchors, four openings for the jacks were cut through the concrete bridge deck. The jacks were hinge connected to the steel loading beams at their top ends and attached to the anchor assembly for the rock anchors at their lower ends. The rock anchors were drilled and grouted approximately 75 ft (23 m) into the ground, 20 ft (6 m) of which were in sound rock. Each rock anchor was capable of resisting a load of 500 kips (2225 kN), which was equal to the capacity of the loading beams.

Each loading beam consisted of two 27 x 114 wide flange beams placed on a roller support at one end and a hinged support at the other. The beams delivered the loads through 2 in. (51 mm) thick steel plates to concrete pedestals located over the webs to give a longitudinal bending type failure. The loads were monitored by separate pressure gages for each jack and verified through strain readings on each ram.

Instrumentation

The bridge was instrumented to monitor deflections, transverse rotations, change in alignment, surface strains in the concrete and forces in diagonal and anchor tendons.

Deflections and Rotations

Deflections and rotations for all load increments were measured using six dial gages with two placed at each end and two placed at midspan. All dial gages measured the displacements in a direction perpendicular to the bottom surface of the girder.

After the girder started yielding, the deflections were measured with an engineer's level, which was set up at a

Fig. 8. The loading frame of the bridge.

distance from the girder, and two level rods, which were permanently mounted at the midspan of the girder.

Strains at Midspan

Strains at the middle of Segment 9B were measured at each load increment using metal foil electrical resistance strain gages. This segment, which is at midspan, was chosen because of the large bending moment at that location. The strain gages were placed on the upper surface, the lower surface, and both sides of the bridge girder as shown in Fig. 9. Only longitudinal gages were used since bending was of primary interest. All strains were used with a Model P-350 Budd Strain Indicator using a half-bridge circuit with temperature compensation gages.

Testing Procedure

A crack survey was made for the outside and inside of the girder before overload testing began. Most of these cracks were caused by temperature and shrinkage. They were traced with black felt-tipped pens to differentiate them from those caused by live load.

The load was applied in increments of 100 kips (445 kN), one increment each day. After each increment of loading, the bridge was completely unloaded and reloaded incrementally in the next day of testing. The testing of the bridge was completed in 9 days. For a typical day of testing, the following steps were carried out:

1. The pressure on the hydraulic rams was released and the steel loading beams were lifted up until there was no contact between the loading beams and bearing points on the concrete pedestals.
2. Initial readings were taken at zero load for strains, deflections, horizontal offsets, and elevations of the deflection points on top of the girder.
3. The four rams were activated by an electric pump, and the pressure read-

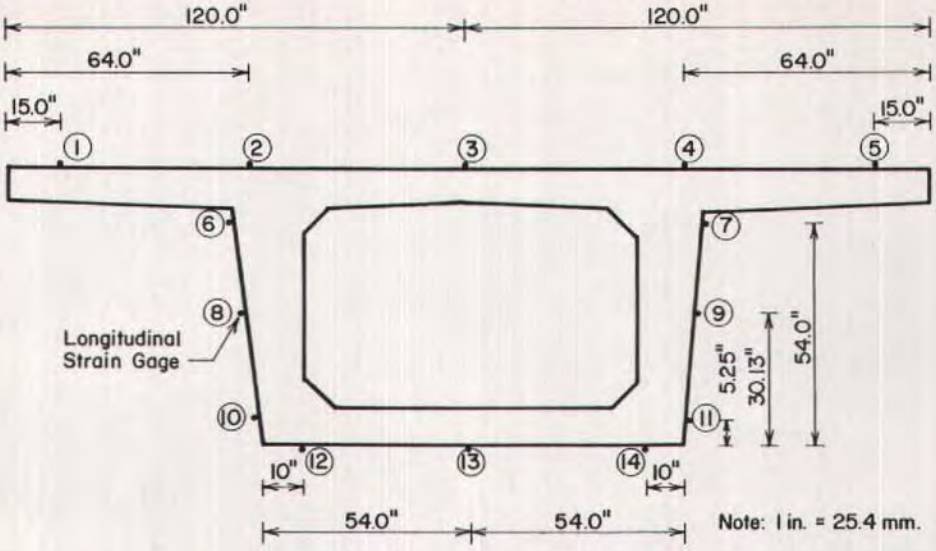

Fig. 9. Locations of strain gages at middle of Segment 9.

ings were adjusted until the load level of the previous day was obtained.

4. Readings of strain gages, dial gages, horizontal offsets, and level rod readings were taken for the applied load level.

5. Cracks were cracked, traced with red felt-tipped pens, identified with the load at which they formed, and recorded. Hand magnifying lenses were used in tracing the ends of the cracks.

6. On the next day of testing, Steps 1 to 5 were repeated, except that the load in Step 3 was increased by 100 kips (445 kN).

Steps 1 to 4 were carried out before sunrise in order to minimize the effect of temperature on the readings, then the crack survey was made during the day with the live load still on the girder.

The bridge was loaded to failure on the last day of testing. Ultimate load was defined by crushing of the concrete after the prestressing reinforcement had yielded and gone into the strain hardening range. After careful examination, there was no evidence of any shear or bond failures.

COMPARISONS OF TEST RESULTS WITH THEORETICAL VALUES

The main purpose of this testing was to study the elastic and inelastic behavior of Girder B. Here, the experimental results are reported and compared with the theoretical values. The tests focused mainly on the determination of experimental deflection and strains from which the stresses were determined. Theoretical results were obtained by the finite element method and by the standard theoretical flexural analysis of prestressed concrete structures. Numerous comparisons were made between observed and calculated quantities, but only a few will be reported here. More comparisons are available in a report by McClure, West, and Abdel-Halim.[12]

Deflections at Midspan

To obtain the total experimental deflection at any load, the permanent set

was added to the measured deflection. This was necessary so that all experimental deflections were measured from the same origin. Finite element deflections were obtained by subtracting the deflections due to load case 2 from load case 1 (see Fig. 7). The standard theoretical analysis procedure for prestressed concrete structures was used to calculate curvature at different load levels. Theoretical deflections were calculated by loading the conjugate beam with the curvature diagram.

The experimental and theoretical midspan deflections are shown in Fig. 10. The figure shows good agreement between finite element and observed deflections with the finite element model showing less stiffness than the real structure. That is, under a given load, the simulated structure deforms more than the actual structure.

Fig. 10 also shows the results of the standard analysis for prestressed concrete beams which shows good agreement with experimental values up to first yielding. The remaining part of the curve was defined by two points. The first point was the first yielding of the bars and the second point was the ultimate condition assuming that concrete fails by crushing when the compression strain reaches a value of 0.003. In this part of the curve, the theoretical deflections are much larger than the experimental ones.

Table 2 shows the observed, finite element and the standard calculated values for loads and deflections at first cracking, first yielding of bars, and at bridge failure. The first yielding load for all solutions was taken to be equal to the theoretical yielding load, and the corresponding deflections were compared accordingly. The percentage differences between the observed and theoretical values are also shown in Table 2.

Longitudinal Stresses/Strains at Midspan

Finite element stresses were obtained

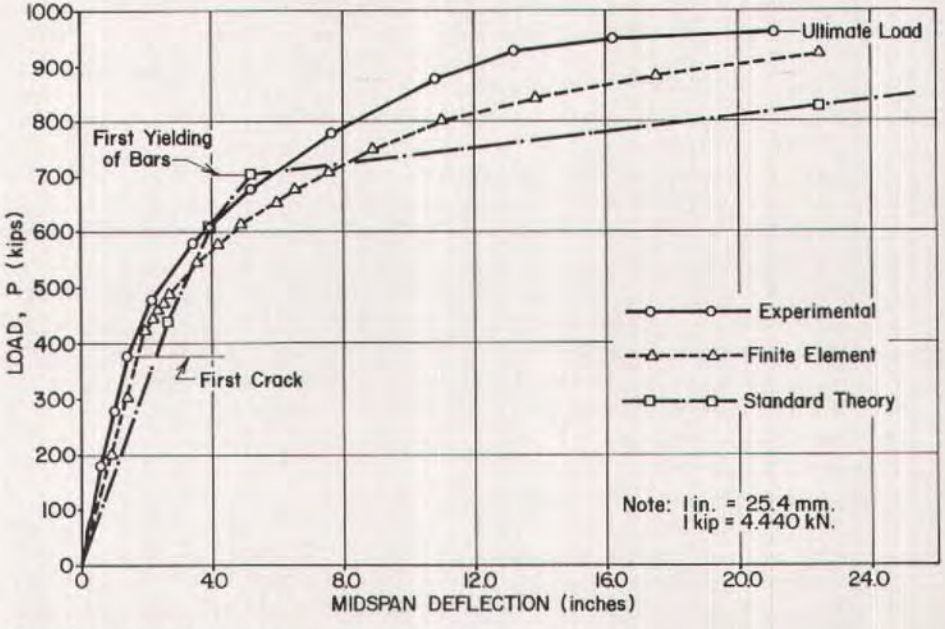

Fig. 10. Load-deflection diagrams of Girder B.

Table 2. Observed, finite element, and calculated values of loads and deflections.

Stage	Load and deflection	Observed values	Finite element values	Percent difference	Standard calculated values	Percent difference
First cracking	Load (kips)	376.0	420.0	+11.70	439.0	+16.76
	Deflection (in.)	1.49	2.01	+34.90	2.79	+87.25
First yielding	Load (kips)	700.0	700.0	0.00	700.0	0.00
	Deflection (in.)	6.00	7.68	+28.00	5.29	−11.83
Failure	Load (kips)	955.0	920.0	−3.66	901.0	−5.65
	Deflection (in.)	21.27	22.10	+3.90	43.49	+104.47

Note: 1 in. = 25.4 mm; 1 kip = 4.448 kN.

Table 3. Observed, finite element and calculated strains at top surfaces.

Applied load (*P*) (kips)	Observed strains (μ in./in.)	Finite element strains (μ in./in.)	Percent difference	Calculated strains (μ in./in.)	Percent difference
439	−254	−302	+18.90	−350	+37.80
600	−359	−509	+41.78	−521	+45.13
700	−449	−616	+37.19	−630	+40.31

Note: 1 kip = 4.448 kN.

by subtracting the stresses of load case 2 from the stresses of load case 1 (see Fig.7). Then the longitudinal strains were calculated using the generalized Hooke's law for a three-dimensional state of stress. Here again, the permanent set strains should be added to the measured strains in order to obtain the absolute surface strains which should be compared with the finite element strains. However, permanent set strains were not measured, and this was one of the main reasons for the deviation in strain results between the finite element analysis and test results.

A comparison of measured and finite element strains did show fair agreement up to first yielding where permanent set strains were small but did show a deviation of results above first yielding where permanent set strains were relatively large. Strains increased almost linearly up to the first cracking load of 376 kips (1670 kN). At a load of 476 kips (2120 kN), the strain gages located near the bottom became inoperative due to cracks developing.[12,13]

A sample for the experimental and finite element strains obtained is shown by Fig. 11 at a load on the bridge equal to 476 kips (2120 kN), which is a load below first yielding. The figure shows a reasonable agreement between observed and finite element strains. The trend observed for deflections is sustained here; that is, the experimental results are smaller than the finite element results.

Based on the standard theoretical analysis, compression strains at the top surface of the girder were calculated at loads of 439, 600, and 700 kips (1950, 2670, and 3110 kN). These strains were compared with the average compression

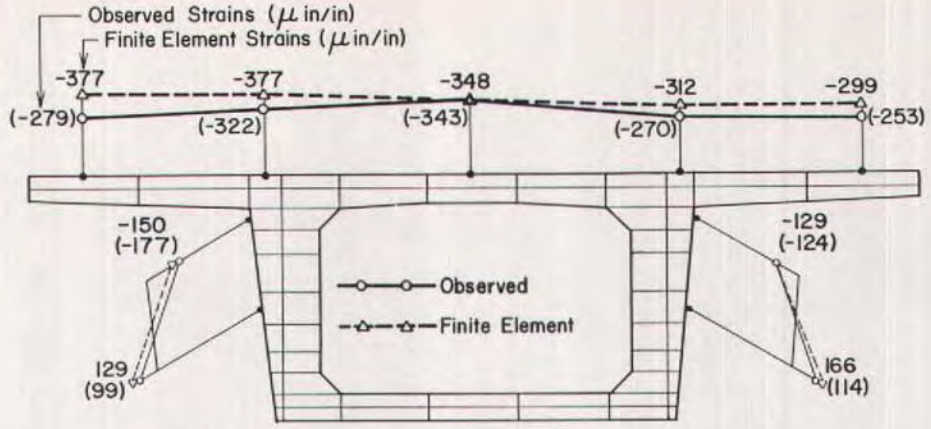

Fig. 11. Longitudinal surface strains at middle of Segment 9 for load of 476 kips (2120 kN).

strains obtained experimentally and by the finite element method. The results are shown in Table 3. This table indicates that the finite element method gives better agreement with the observed results than does the standard theoretical analysis. The same indication was obtained by the load-deflection response (see Fig. 10). The percentage differences between the observed and theoretical values are also shown in Table 3.

Cracking and Failure of the Bridge

In the first and second days of testing, up to load P = 276 kips (1228 kN), there was no visible cracking on the bottom surface of the bridge. In the third day of testing, at load P = 376 kips (1672 kN), the first visible cracking was observed at the bottom surface between the points of loading. As the load was increased, cracks increased in number, and those between the points of loading widened and extended toward the compression zone. In the transverse direction, it was noticed that cracks began at the inner side of the girder and progressed gradually toward the outer side.

Nothing unusual was noticed until the eighth day of testing, at load P = 876 kips (3876 kN), when two loud sounds were heard at different times and the pressure gage readings dropped down slightly. It sounded like a strand or bar tendon had broken each time. At this load, the cracks at Joints 8 and 9 opened widely and extended upward toward the top slab.

In the last day of testing, at load P = 945 kips (4203 kN), two events occurred: first, a noise was heard and the deflection increased suddenly by 0.25 in. (6.35 mm); second, two loud sounds, simlar to those which occurred at P = 876 kips (3896 kN), were heard. Again, deflection increased suddenly by another 0.25 in. (6.35 mm). Pressure reading started to fall off, but reached a constant value. As the load was slightly increased to the failure load of P = 955 kips (4250 kN), the crack at one of the middle joints (Joint 8) opened widely and the concrete in the compression zone crushed and spalled on the surface. The mode of failure of the bridge is shown in Fig. 12. Upon inspection of Joint 8, it was found that all the strands were broken and the solid bars were holding the bridge in place.

The finite element load at first cracking was estimated at P = 420 kips (1868 kN) which is 11.70 percent larger than the observed value. The cracking load

(a) Plan (bottom surface)

(b) Elevation

Fig. 12. Mode of failure of the bridge.

calculated from conventional theory was P = 439 kips (1953 kN) which is 16.76 percent larger than the observed value. Also, the finite element load at failure was estimated at P = 920 kips (4092 kN) which is 3.66 percent smaller than the observed value. The failure load calculated from conventional theory using strain compatibility was P = 901 kips (4000 kN) which is 5.65 percent smaller than the observed value. These values are given in Table 2.

With the failure load of 955 kips (4250 kN) on the girder, the ultimate live load moment in the midspan section between points of loading was 26,024 kip-ft (35, 288 kN•m) for the 121 ft (36.9 m) simply supported span. If Girder B takes two lanes of AASHTO HS20-44 design load plus 20.3 percent for impact, the design live load moment would be:

2 (1901.3)(1.203)

= 4575 kip-ft (6204 kN•m)

The load factor for the live load would then be 26,024/4,575 = 5.69, assuming a load factor for dead load equal to 1.00.

For a dead load of 4.514 kips/ft (65.86 kN/m), the maximum dead load moment at midspan would be:

$1/8\,(4.514)(121)^2$

= 8261 kip-ft (11,201 kN•m)

The load factor for live load would then be [34,285 - 1.3(8261)]/4575 = 5.15 if the load factor for dead load was considered to be 1.3 as recommended by AASHTO. Both of these live load factors exceed the 2.17 value recommended by the current AASHTO specifications for load factor design.[14] The reason for the excessive load factor for live load is that extra steel was required in the girder to satisfy allowable stresses under unfactored loads.

Crack Patterns

Sketches were drawn for the crack patterns for the inside and outside of

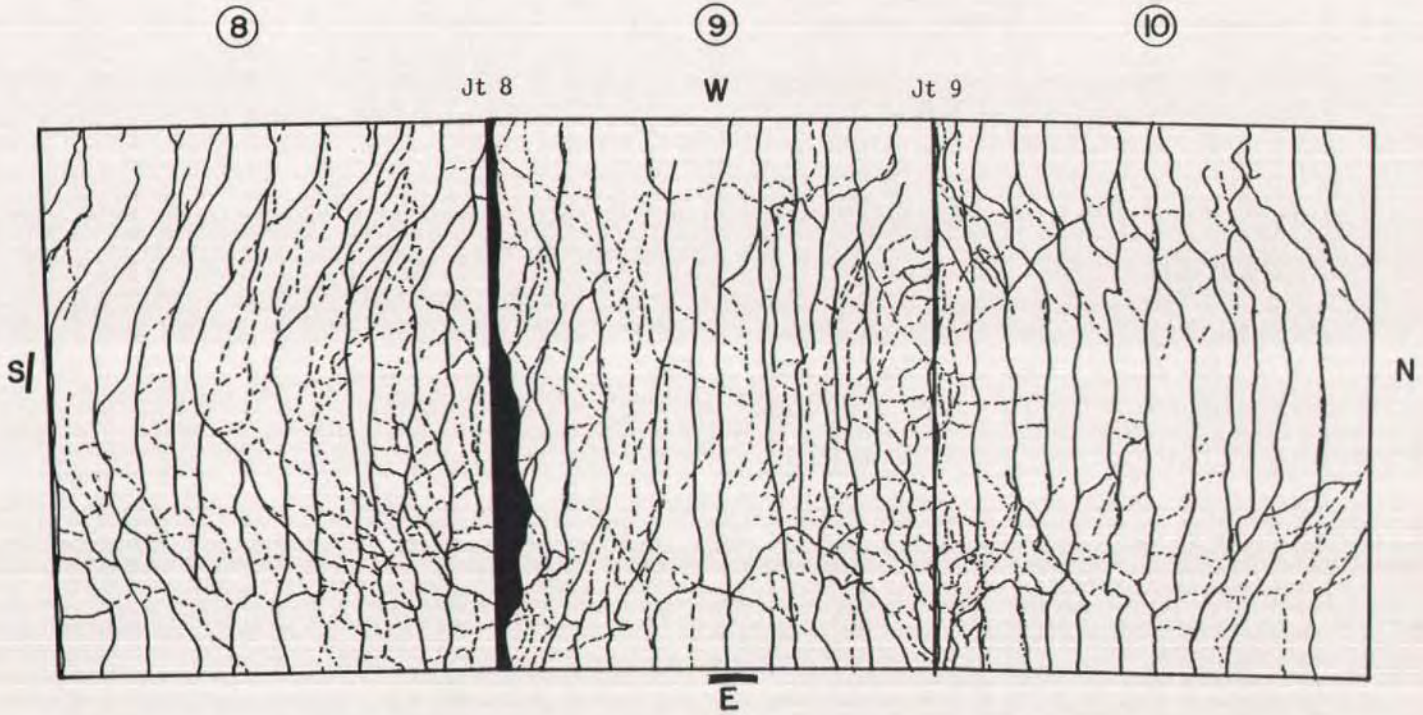

Fig. 13. Outside crack pattern for bottom of Girder B at failure.

Girder B, at load P = 776 kips (3453 kN), and at failure. Fig. 13 shows the outside crack pattern for the bottom of Girder B at failure for the three segments nearest midspan. At failure most of the cracking occurred on these three segments. Dotted lines on this figure represent the cracks that occurred after load P = 776 kips (3450 kN) up to failure. The thicker line indicates the joint that opened wide and caused the failure.

It should be noted that all cracks between the points of loading were flexural cracks, and as one goes farther from the points of loading, the cracks bend more in a diagonal direction. These are known as flexure-shear cracks. It can be noted also that at the maximum load level, there was a tendency in segmental structures to concentrate strains or curvatures and yielding of tendons at one or more joint locations. This is because the mild reinforcing bars are not continuous across the joint. For Girder B, at load P = 945 kips (4200 kN), Joints 8 and 9 were wide open, and strain concentrations were approximately equal at these joints. At the failure load of P = 955 kips (4250 kN), however, Joint 9 started to close, all strain concentrations appeared at Joint 8, and a flexural type failure occurred at this joint.

CONCLUSIONS

The material reported in this paper does not cover all of the topics that were covered in the research study. More comprehensive findings have been reported by McClure, West, and Abdel-Halim.[12,13] The following conclusions can be made as a result of this study:

1. The results of the three-dimensional finite element analysis, deflections and stresses (strains), which used the Kostovos and Newman material model for concrete, compared reasonably well with experimental values in the elastic and the post-cracking ranges.

2. The experimental deflections and strains (stresses) at midspan from longitudinal bending were always less than the corresponding finite element values. This indicates that the actual structure is stiffer than that predicted by theory.

3. Cracking, first yielding, and ultimate loads were found to be in good agreement with their respective finite element values.

4. The general analysis approach based upon the finite element method gives a great amount of information on deflections, strains, stresses, and forces in the prestressing steel, which can be used in judging the behavior of bridges if the structure is properly modeled.

5. Theoretical deflection and strains (stresses) obtained by the standard analysis procedure for prestressed concrete structures were found to agree closely with observed values up to first yielding, but after first yielding agreement was not good.

6. The standard prestressed analysis can be used to calculate loads, deflections, and strains (stresses), up to the first yielding of the steel, but after first yielding, calculations are not reliable. The ultimate load still can be conservatively predicted by these standard methods with a good degree of accuracy.

7. A bending type failure occurred between the points of loading. There was no sign of a shear type distress near the ends. The bridge had an adequate but conservative factor of safety against failure.

8. The standard prestress analysis was used in the design of the experimental segmental bridge for longitudinal bending, shear, and torsion. For future designs of this type, the standard prestress analysis can be safely used. However, an analysis based on the finite element method would also give safe results which are less conservative. Some economy in design might be achieved by using the finite element method of analysis in the design.

ACKNOWLEDGMENT

This study covers a portion of a major 6-year investigation on an experimental segmental bridge which was conducted at the Pennsylvania Transportation Institute located at The Pennsylvania State University. The study was sponsored and funded by the Pennsylvania Department of Transportation and the Federal Highway Administration. The contents of this paper reflect the views of the authors who are responsible for the facts and the accuracy of the data. The contents do not necessarily reflect the official views or policies of the sponsors.

REFERENCES

1. Koretzky, H. P., and Tscherneff, A. T., *Final Report for Research Project No. 72-9 on the Design of an Experimental Post-tensioned Segmental Concrete Box Girder Bridge*, Pennsylvania Department of Transportation, Publication No. 118, September 1974.
2. Chen, W. F., *Plasticity in Reinforced Concrete*, McGraw-Hill Book Company, New York, N.Y., 1982.
3. Kostovos, M. D., and Newman, J. B., "Generalized Stress-Strain Relations for Concrete," *Journal of the Engineering Mechanics Division*, American Society of Civil Engineers, V. 104, No. EM4, August 1978, pp. 845-856.
4. Kostovos, M. D., and Newman, J. B., "A Mathematical Description of the Deformational Behavior of Concrete Under Complex Loading," *Magazine of Concrete Research* (London), V. 31, No. 107, June 1979, pp. 77-90.
5. Kostovos, M. D., "A Mathematical Description of the Strength Properties of Concrete Under Generalized Stress," *Magazine of Concrete Research* (London), V. 31, No. 108, September 1979, pp. 151-158.
6. Kostovos, M. D., and Newman, J. B., "Behavior of Concrete Under Multiaxial Stress," *ACI Journal*, V. 74, No. 9, September 1977, pp. 443-446.
7. Liu, T. C. Y., Nilson, A. H., and Slate, F. O., "Biaxial Stress-Strain Relations for Concrete," *Journal of the Structural Division*, American Society of Civil Engineers, V. 98, No. ST5, Proceedings Paper 8905, May 1972, pp. 1-25-1934.
8. Hand, F. R., Pecknold, D. A., and Schnobrich, W. C., "A Layered Finite Element Nonlinear Analysis of Reinforced Concrete Plates and Shells," *Structural Research Series No. 389*, Civil Engineering Studies, University of Illinois, Urbana—Champaign, August 1972.
9. Bathe, K. J., Wilson, E. L., and Paterson, F. E., "SAPIV—A Structural Analysis Program for Static and Dynamic Analysis of Linear Structural Systems," *EERC Report No. 73-11*, College of Engineering, University of California, Berkeley, June 1973, Revised April 1974.
10. Nilson, A. H., *Design of Prestressed Concrete*, John Wiley & Sons, New York, 1978.
11. Lin, T. Y., and Burns N. H., *Design of Prestressed Concrete Structures*, Third Edition, John Wiley & Sons, New York, N.Y., 1981.
12. McClure, R. M., West, H. H., and Abdel-Halim, M., *Overload Testing of an Experimental Segmental Bridge*, Interim Report, Project 75-3, The Pennsylvania Transportation Institute, University Park, Pennsylvania, July 1982.
13. Abdel-Halim, M. A. H., *Nonlinear Analysis of a Segmental Concrete Bridge by Finite Element Method*, PhD Thesis, The Pennsylvania State University, March 1982.
14. American Association of State Highway and Transportation Officials, *Standard Specifications for Highway Bridges*, Washington, D.C., 1983.

NOTE: Discussion of this article is invited. Please submit your comments to PCI Headquarters by August 1, 1988.